Progress In Electromagnetics Research, PIER 83, 43–54, 2008

RESISTANCES AND INDUCTANCES EXTRACTION USING SURFACE INTEGRAL EQUATION WITH THE ACCELERATION OF MULTILEVEL GREEN FUNCTION INTERPOLATION METHOD

P. Zhao and H. G. Wang

The Electromagnetics Academy at Zhejiang University
Zhejiang University
Hangzhou 310058, China

Abstract—In this paper, we consider the resistances and inductances extraction from finite conducting metals. To remedy the weakness of volume integral equation, we extend the usage of a surface integral equation method from analyzing finite conducting rectangular wire strip to analyzing arbitrarily shaped geometry. Moreover the multilevel Green function method (MLGFIM) with a complexity of $O(N)$ is employed to accelerate the matrix-vector multiplications in iterations. The numerical results shows the efficacy of the proposed method.

1. INTRODUCTION

Conventional surface integral equation (SIE) solver can simulate the currents flowing on the perfect electric conducting (PEC) metal. When we extract inductance and resistance of metal, we can view this kind of problems as low frequency electromagnetic problems [1]. A lot of methods [2–4] have been developed to solve this kind of problems. However, for a metal with finite conductivity, because the waves will penetrate the surface of it, conventional SIE can not be directly used any more. In [5], a SIE method is developed considering the skin effect. However, it is restricted for solving rectangular wire strip problems, because when the upper and lower surfaces of the conductor are not parallel, the internal E fields can not be simply expressed as (2) of [5], viz., $E = E^{+}e^{-\gamma z} + E^{-}e^{+\gamma z}$, where γ is the propagation constant defined in [5]. Recently, we have developed the volume loop integral equation (VLIE) method [6]. This method is accurate for calculating the inductance and resistance of the metal when its size of cross section is comparable to the skin depth. However, when the metal is relatively

thick, viz., the size of the metal becomes much greater than the skin depth, to obtain an accurate resistance using VLIE, the high density volume mesh to model skin effect at RF frequency correctly make the solution very computationally expensive, viz., the unknowns will increase to an unmanageable number for our computer.

There exist several fast algorithms for matrix-vector multiplication that can be used to enhance the efficiency of the solution, such as fast multipole method (FMM) [7–9], conjugate gradient fast Fourier transform (CGFFT) [10, 11], precorrected FFT (PFFT) [12], the sparse matrix/canonical grid (SMCG) method [13], adaptive integral method (AIM) [14], and MLGFIM [15, 16] and so on. Among them, FMM is a fast algorithm with $O(N)$ complexity, CGFFT, PFFT, SMCG, and AIM are FFT based methods with $O(N \log N)$ complexity, while MLGFIM is based on a hierarchical structure which is similar to FMM but using the Green's function matrix interpolation method with QR [17] factorization technique. This method has a complexity of $O(N)$ [15].

To remedy these, we extend the usage of (6) in [5] that is restricted in the particular structure to solve the relatively thick metal problems with complex geometries. Here we call it the finite conductivity surface integral equation (FCSIE). Though the FCSIE is derived from the Volume Integral Equation, it is similar to the Electric Field Integral Equation Method (EFIE) with Impedance Boundary Condition (IBC) Approximations that is always used in solving the EM scattering problems [18, 19]. However, here we use it for quasistatic inductance extraction problems. For the source voltage excitation and the source loop basis functions, we use the shortest path algorithm as that in [20] to find the source path. To accelerate the FCSIE, the recently developed MLGFIM algorithm is also employed. The numerical results of spiral inductors and a sphere bump in this paper show the validity and efficiency of this method.

2. SURFACE INTEGRAL EQUATION FOR ARBITRARILY SHAPED FINITE CONDUCTING METAL

For finite conducting metal problems in integrated circuits, the volume mixed potential electric field equation can be used:

$$\mathbf{E}(\mathbf{r}) = i\omega\mu \int_{\Omega} dv' \frac{e^{ikR}}{4\pi R} \mathbf{J}_{eq}(\mathbf{r}') - \nabla\phi \tag{1}$$

where $\mathbf{E}(\mathbf{r})$, $\mathbf{J}_{eq}(\mathbf{r}')$, ϕ, ω, μ and k are the total electric field, volume equivalent current density, scalar potential, angular frequency, free space permeability and free space wavenumber, respectively. R is defined as $|\mathbf{r}-\mathbf{r}'|$. This equation is used in [6] for inductance extractions. However, when the frequency is very high and thus the skin depth becomes very shallow, the currents are almost restricted in a very thin shell of the metal. Consequently, the tetrahedron mesh used in [6] can no longer efficiently model the skin effects.

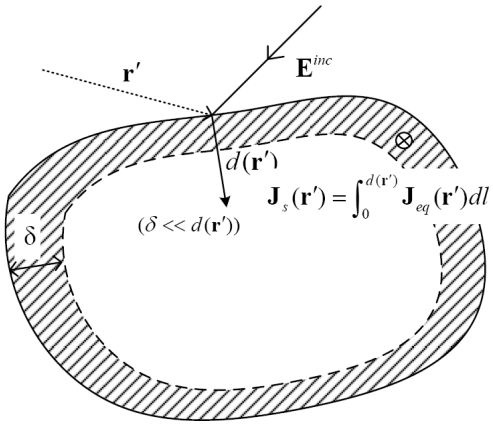

Figure 1. Plane wave impinges on the conductor.

Suppose a plane wave impinges on the surface of a relatively thick metal (Figure 1), where $d(\mathbf{r}')$ is the depth from the surface point $\mathbf{r}'$ and it is greatly larger than the skin depth, $\mathbf{J}_s$ is the surface currents. Here, we consider the integration of the volume current density along the skin depth direction and view it as the approximated surface currents. Thus, (1) can be rewritten as a surface integral equation:

$$\mathbf{E}(\mathbf{r}) \approx i\omega\mu \int_s ds' \frac{e^{ikR}}{4\pi R}\mathbf{J}_s(\mathbf{r}') - \nabla\phi \tag{2}$$

where

$$\mathbf{J}_s(\mathbf{r}) = \int_0^{d(\mathbf{r})} \mathbf{J}_{eq}(\mathbf{r})dl = \int_0^{d(\mathbf{r})} \sigma\mathbf{E}(\mathbf{r})e^{i\sqrt{i\omega\mu\sigma}l}dl \approx \mathbf{E}(\mathbf{r})\sqrt{\frac{i\sigma}{\omega\mu}} \tag{3}$$

where σ is the conductivity of the metal.

Substituting (3) into (2) gives

$$\sqrt{\frac{\omega\mu}{i\sigma}}\mathbf{J}_s - i\omega\mu \int\limits_s ds' \frac{e^{ikR}}{4\pi R}\mathbf{J}_s(\mathbf{r}') = -\nabla\varphi. \tag{4}$$

Though (4) is similar to (6) in [5], it is derived from the volume integral equation (VIE) without the restriction $E = E^+e^{-\gamma z} + E^-e^{+\gamma z}$. It can be viewed as an extension of (6) in [5] and a complementary of VIE method, and used to solve the relatively thick metal problems with complex geometries. It also can be viewed as a special form of the EFIE with IBC. (The wave impedance in the good conductor equals $\eta_0\eta_s \approx \sqrt{\frac{\omega\mu}{i\sigma}}$ [21]. Thus the EFIE with IBC approximation in [18, 22] will be degenerated to (4).) However, it is straightforwardly derived from the volume integral equation, and is used in solving for the quasistatic inductance extraction problems here.

3. SURFACE LOOP EXPANSION AND MLGFIM ACCELERATION

Choosing loop basis functions $\{\mathbf{o}_m(\mathbf{r})\}_{m=1}^{N_L}$, (where N_L is the number of loop bases) [23–25] and applying the Galerkin method, we can convert (4) to

$$\bar{\bar{Z}}' \cdot \bar{I} = \bar{V} \tag{5}$$

where the (m, n)-th entry of $\bar{\bar{Z}}'$ is

$$Z'_{m,n} = \sqrt{\frac{\omega\mu}{i\sigma}} \int\limits_{s_n} ds \mathbf{o}_m(\mathbf{r}) \cdot \mathbf{o}_n(\mathbf{r}) - i\omega\mu \int\limits_{s_m} ds \int\limits_{s_n} ds' \mathbf{o}_m(\mathbf{r}) \cdot \frac{e^{ikR}}{4\pi R} \cdot \mathbf{o}_n(\mathbf{r}') \tag{6}$$

and

$$V_n = -\int\limits_{s_n} ds \mathbf{o}_n(\mathbf{r}) \cdot \nabla\phi. \tag{7}$$

Because $\mathbf{o}_m(\mathbf{r})$ is the combination of the RWG bases, (6) can also be rewritten as

$$Z'_{m,n} = \sum_{p=1}^{N}\sum_{q=1}^{N} P_{m,p}P_{n,q}Z_{p,q} \tag{8}$$

where

$$Z_{p,q} = \sqrt{\frac{\omega\mu}{i\sigma}} \int\limits_{s_q} ds \mathbf{f}_p(\mathbf{r}) \cdot \mathbf{f}_q(\mathbf{r}) - i\omega\mu \int\limits_{s_p} ds \int\limits_{s_q} ds' \mathbf{f}_p(\mathbf{r}) \cdot \frac{e^{ikR}}{4\pi R} \cdot \mathbf{f}_q(\mathbf{r}') \tag{9}$$

where $\mathbf{f}_p(\mathbf{r})$ is the p-th RWG basis [26–28] and N is the number of RWG bases used to model the problem. Thus (5) can be rewritten as

$$\bar{\bar{P}} \cdot \bar{\bar{Z}} \cdot \bar{\bar{P}}^T \cdot \bar{I} = \bar{V} \tag{10}$$

where $\bar{\bar{P}}$ has the same definition as in [6].

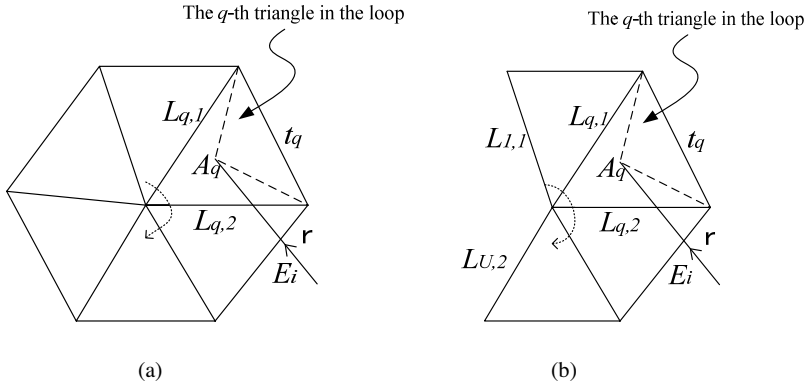

Figure 2. The support of a surface loop basis function.

The surface loop bases are classified into the closed loop bases and the unclosed loop bases whose supports are shown in Figure 2(a) and (b), respectively. In triangle q of a loop basis function support, the loop basis function can be expressed as $\mathbf{I}_q = \frac{\mathbf{t}_q}{2\Delta_q}$, where Δ_q is the area of triangle in RWG bases and $\mathbf{t}_q$ is defined in Figure 2. Similarly as [6], after some operation in (11), we can obtain that (7) becomes zero if the support of the loop basis function is closed and otherwise it equals the unclosed loop voltage.

$$\begin{aligned} V &= -\sum_{q=1}^{U} \int_{s_q} ds \mathbf{I}_q(\mathbf{r}) \cdot \nabla\phi \\ &= -\sum_{q=1}^{U} \left\{ \int_{T_q} ds \nabla \cdot [\mathbf{I}_q(\mathbf{r})\phi] - \int_{T_q} ds\phi \nabla \cdot \mathbf{I}_q(\mathbf{r}) \right\} \\ &= -\sum_{q=1}^{U} \oint_{T_q} dl \cdot \mathbf{I}_q(\mathbf{r})\phi \end{aligned}$$

$$
\begin{aligned}
&= -\sum_{q=1}^{U}\left\{\int\limits_{L_{q,1}} dl\cdot\mathbf{t}_q(\mathbf{r})\phi/2\Delta_q + \int\limits_{L_{q,2}} dl\cdot\mathbf{t}_q(\mathbf{r})\phi/2\Delta_q\right\}\\
&= -\sum_{q=1}^{U-1}\left\{\int\limits_{L_{q+1,1}} dl\cdot\mathbf{t}_{q+1}(\mathbf{r})\phi/2\Delta_{q+1} + \int\limits_{L_{q,2}} dl\cdot\mathbf{t}_q(\mathbf{r})\phi/2\Delta_q\right.\\
&\quad\left. + \int\limits_{L_{1,1}} dl\cdot\mathbf{t}_1(\mathbf{r})\phi/2\Delta_1 + \int\limits_{L_{U,2}} dl\cdot\mathbf{t}_U(\mathbf{r})\phi/2\Delta_U\right\}\\
&= -\left\{\sum_{q=1}^{U-1}[h_{q,2}/2\Delta_q - h_{q+1,1}/2\Delta_{q+1}]\int\limits_{L_{q,2}} dl\phi\right.\\
&\quad\left. - h_{1,1}/2\Delta_1\int\limits_{L_{1,1}} dl\phi + h_{U,2}/2\Delta_U\int\limits_{L_{U,2}} dl\phi\right\}\\
&= -\left(0-\phi(\xi)|_{\xi\in L_{1,1}} + \phi(\xi)|_{\xi\in L_{U,2}}\right)\\
&= \begin{cases} 0, & \text{if the loop is closed}\\ \phi(\xi)|_{\xi\in L_{1,1}} - \phi(\xi)|_{\xi\in L_{U,2}}, & \text{other else}\end{cases}
\end{aligned}
\tag{11}
$$

where U is the number of triangles in the loop basis function, $h_{q,1}$ and $h_{q,2}$ are the height respectively perpendicular to lengths $L_{q,1}$ and $L_{q,2}$ that are shown in Figure 2.

When we can find a path of interconnected triangles between the two ends of this conductor, an unclosed source loop basis function is found, that can be used for the support of the conductor, viz. impose the voltage between its two ends.

The major difference between (10) here and (9) in [6] is that the integrations in $Z_{p,q}$ are on surface now. Hence, we can use the MLGFIM program developed in [6] by replacing the volume integrations in [6] with the surface integrations here.

We know that the integral $\int\limits_{s_q} ds\mathbf{f}_p(\mathbf{r})\cdot\mathbf{f}_q(\mathbf{r})$ isn't zero when test function and basis function is overlapped, when we use MLGFIM [15, 16] for far field computation, the test function and basis function is not in the same cube, thus, the integral result is zero. So the far field entries in $\bar{\bar{Z}}$ can be simplified as

$$
Z_{p,q} = -i\omega\mu\int\limits_{s_p} ds\int\limits_{s_q} ds'\mathbf{f}_p(\mathbf{r})\cdot G_0(\mathbf{r},\mathbf{r}')\cdot\mathbf{f}_q(\mathbf{r}') \tag{12}
$$

where $G_0(\mathbf{r},\mathbf{r}') = \frac{e^{ikR}}{4\pi R}$. The integral $\int\limits_{s_p} ds \int\limits_{s_q} ds' \mathbf{f}_p(\mathbf{r}) \cdot G_0(\mathbf{r},\mathbf{r}') \cdot \mathbf{f}_q(\mathbf{r}')$ is decomposed into x, y and z parts, and each part can be written as

$$\hbar_{pq} = \int\limits_{S_p} ds \int\limits_{S_q} ds' \tau_p(\mathbf{r}) \tau_q(\mathbf{r}') \mathbf{G}_0(\mathbf{r},\mathbf{r}') \tag{13}$$

It has been mentioned before, source point and field point are in two well-separated cube $\mathbf{G}_m$ and $\mathbf{G}_n$, we can obtain $\mathbf{G}_0(\mathbf{r},\mathbf{r}')$ by interpolation technique, viz.,

$$\begin{aligned} \mathbf{G}_0(\mathbf{r},\mathbf{r}') &= \sum_{i=1}^{K}\sum_{j=1}^{K} \omega_{m,i}(\mathbf{r}) \omega_{n,j}(\mathbf{r}') \mathbf{G}_0\left(\mathbf{r}_{\mathbf{G}_m,i}, \mathbf{r}_{\mathbf{G}_n,j}\right) \\ &= \bar{\omega}_m^T(\mathbf{r}) \cdot \bar{\bar{\mathbf{G}}}_{m,n} \cdot \bar{\omega}_n(\mathbf{r}') \end{aligned} \tag{14}$$

where $\omega_{m,i}(\mathbf{r})$, $\omega_{n,j}(\mathbf{r}')$, $\mathbf{G}_0(\mathbf{r}_{\mathbf{G}_m,i}, \mathbf{r}_{\mathbf{G}_n,j})$ and K have been defined in [6]. Substituting (14) into (13) gives

$$\begin{aligned} \hbar_{pq} &= \int\limits_{S_p} ds \int\limits_{S_q} ds' [\tau_p(\mathbf{r}) \tau_q(\mathbf{r}')] \bar{\omega}_m^T(\mathbf{r}) \cdot \bar{\bar{\mathbf{G}}}_{m,n} \cdot \bar{\omega}_n(\mathbf{r}') \\ &= \left[\int\limits_{S_p} ds \tau_p(\mathbf{r}) \bar{\omega}_m^T(\mathbf{r})\right] \bar{\bar{\mathbf{G}}}_{m,n} \left[\int\limits_{S_q} ds' \tau_q(\mathbf{r}') \bar{\omega}_n(\mathbf{r}')\right] \\ &= \bar{v}_{m,p}^T \cdot \bar{\bar{\mathbf{G}}}_{m,n} \cdot \bar{v}'_{n,q} \end{aligned} \tag{15}$$

After we obtain the $\bar{V}$ vector, we will use the MLGFIM, viz., Algorithm 1 [16] without calculating the term for scalar potential, because in the problem of this paper, no scalar potential is needed for building the MoM matrix.

4. NUMERICAL RESULTS

To validate the accuracy and efficiency of our method, some examples are given. First, we give an example of three interconnects structure in integrated circuit to show the accuracy of VLIE [6] in solving thin structures. Second, we compare the results of thick spiral inductor problems using VLIE method with those using FCSIE method to show the advantage of FCSIE in solving thick structures. Moreover, a bump example is given to show the flexibility of solving complex structure. Third, we present frequency responses of a spiral inductor and compare the resistances and inductances with FastHenry [29] to

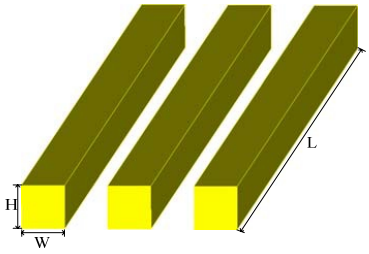

(a)

	R(Ohm)			L(pf)		
FastHenry Results	0.341	0.0142	0.0337	77.8	50.8	39.4
	0.0143	0.361	0.0143	50.8	77.1	50.8
	0.0336	0.0144	0.341	39.5	50.8	77.8
VLIE Results	0.336	0.0139	0.0331	78.3	50.9	39.5
	0.0138	0.360	0.0144	50.8	77.7	50.9
	0.0332	0.0139	0.338	39.4	50.8	78.4

(b)

Figure 3. (a) A three copper interconnects structure ($\sigma = 5.961\times10^7$); (b) Resistances and inductances matrix results($f = 10\,\text{GHz}$.)

show the accuracy of our method. Finally, the memory used and CPU time cost show that the complexity of our algorithm is $O(N)$.

The example in Figure 3(a) is a three copper interconnects structure. We set W and H as 3 microns, and L as 100 microns, because the characteristic sizes of interconnects range from submicron to several microns. From the resistances and inductances results in Figure 3(b), we can see that the differences between the resistances and inductances of FastHenry and that of VLIE method are negligible. That means there is no problem for VLIE method in solving thin structures.

Table 1. The inductances and resistances of the spiral inductors of 2.5 turns and 3.5 turns and the bump in [6]. ($f = 10\,\text{GHz}$).

Examples at 10 GHz	FCSIE-MLGFIM		VLIE [2]		FastHenry [16]	
	R (Ohm)	L (nH)	R (Ohm)	L (nH)	R (Ohm)	L (nH)
2.5 turn spiral inductor	1.223	2.215	1.889	2.229	1.189	2.248
3.5 turn spiral inductor	2.106	4.4	3.296	4.420	1.965	4.487
Bump	0.0621	0.0355		0.0339		

Table 1 shows resistances and inductances of two 2.5 turn and 3.5 turn copper spiral inductors with the size parameters w, t, s, and R being 20, 15, 20, and 100 microns in Figure 4(a). From Table 1, we see that our results agree well with that obtained using FastHenry [29], in contrast, VLIE method can not accurately obtain the resistances

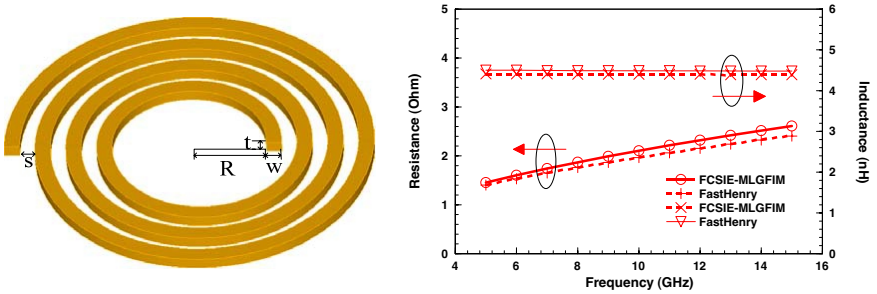

(a) (b)

Figure 4. (a) A 3.5 turns spiral inductor ($\sigma = 5.961 \times 10^7$); (b) Frequency responses of the spiral inductor.

because of the restriction of the mesh density. Our method can also obtain the resistance and inductance of complex object, e.g., the bump in [6], while the Volume-Loop method [6] can only provide the accurate inductance of this bump because the bump is very thick. The inductance result agree well with that using VLIE method.

Figure 4(b) is the frequency response of the spiral inductor. We can see the resistances increase with frequency, while the inductances are unchanged. The inductance results agree well with that obtained using FastHenry. The maximum difference of the resistance results between our data and FastHenry data is less than 10%, which is sufficiently accurate for engineering use.

In Figure 5, we plot the memory requirement and the CPU time

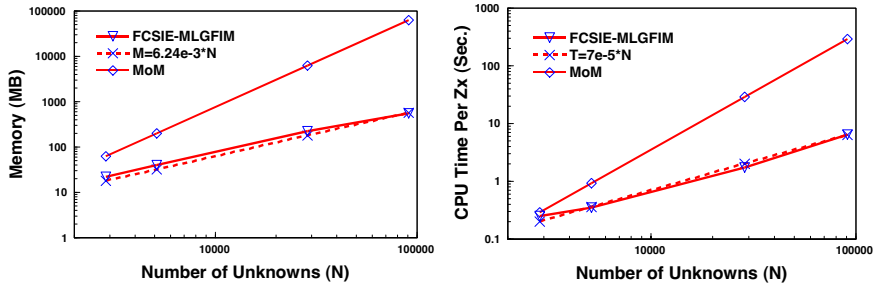

(a) (b)

Figure 5. (a) The memory requirement versus the number of RWG bases; (b) The CPU time used per matrix-vector multiplication versus number of RWG bases.

per matrix-vector multiplication for the bump with different number of RWG basis functions. The predicted values for MoM method is also drawn for comparisons. We see that using MLGFIM can significantly save the memory and time. The complexity of our algorithm is $O(N)$. When the number of RWG basis functions increases, the memory used and time cost will significantly decrease.

5. CONCLUSION

In this paper, the surface integral equation [5] for finite conducting metal is extended to solve for resistances and inductances of metals with complex geometries. The MLGFIM with $O(N)$ complexity is also used to further enhance its efficiency. The numerical examples and the complexity curves show the validity and efficiency of this method.

ACKNOWLEDGMENT

This work was supported by Provincial Nature Science Foundation of Zhejiang, China No. Y105477, National Nature Science Foundation of China No. 60501017.

REFERENCES

1. Venkov, G., M. W. McCall, and D. Censor, "The theory of low-frequency wave physics revisited," *Journal of Electromagnetic Waves and Applications*, Vol. 21, No. 2, 229–249, 2007.
2. Tang, W., X. He, T. Pan, and Y. L. Chow, "Synthetic asymptote formulas of equivalent circuit components of square spiral inductors," *Journal of Electromagnetic Waves and Applications*, Vol. 20, No. 2, 215–226, 2006.
3. Zheng, Q. and H. Zeng, "Multipole theory analysis of 3D magnetostatic fields," *Journal of Electromagnetic Waves and Applications*, Vol. 20, No. 3, 389–397, 2006.
4. Babic, S. I. and C. Akyel, "New mutual inductance calculation of the magnetically coupled coils: thin disk coil-thin wall solenoid," *Journal of Electromagnetic Waves and Applications*, Vol. 20, No. 10, 1281–1290, 2006.
5. Morsey, J. D., V. I. Okhmatovski, and A. C. Cangellaris, "Finite-thickness conductor models for full-Wave analysis of interconnects with a fast integral equation method," *IEEE Trans. Advaced-packaging*, Vol. 27, No. 1, 24–33, Feb. 2004.

6. Wang, H. G. and P. Zhao, "Combining multilevel Green's function interpolation method with volume loop bases for inductance extraction problems," *Progress In Electromagnetics Research*, PIER 80, 225–239, 2008.
7. Rokhlin, V., "Rapid solution of integral equation of classical potential theory," *J. Comput. Phys.*, Vol. 60, 187–207, 1985.
8. Lu, C. C. and W. C. Chew, "A multilevel algorithm for solving boundary integral equations of wave scattering," *Microw. Opt. Tech. Lett.*, Vol. 7, 466–470, Jul. 1994.
9. Song, J. M., C. C. Lu, W. C. Chew, and S. W. Lee, "Fast illinois solver code (FISC)," *IEEE Antennas Propag. Mag.*, Vol. 48, 27–34, Jun. 1998.
10. Sarkar, T. K., E. Arvas, and S. M. Rao, "Application of FFT and the conjugate gradient method for the solution of electromagnetic radiation from electrically large and small conducting bodies," *IEEE Trans. Antennas Propagat.*, Vol. 34, 635–640, May 1986.
11. Zhao, L., T. J. Cui, and W.-D. Li, "An efficient algorithm for EM scattering by electrically large dielectric objects using MR-QEB iterative scheme and CG-FFT method," *Progress In Electromagnetics Research*, PIER 67, 341–355, 2007.
12. Phillips, J. R. and J. K. White, "A precorrected-FFT method for electrostatic analysis of complicated 3-D structures," *IEEE Trans. Comput.-Aided Des. Integr. Circuits Syst.*, Vol. 16, 1059–1072, Oct. 1997.
13. Chan, C. H., C.-M. Lin, L. Tsang, and Y. F. Leung, "A sparse matrix/canonical grid method for analyzing microstrip structures," *IEICE Trans. Electron.*, Vol. E80-C, No. 11, 1354–1359, Nov. 1997.
14. Bleszynski, E., M. Bleszynski, and T. Jaroszewicz, "AIM: Adaptive integral method for solving large-scale electromagnetic scattering and radiation problems," *Radio Sci.*, Vol. 31, 1225–1251, Sept.–Oct. 1996.
15. Wang, H. G., C. H. Chan, and L. Tsang, "A new multilevel Green's function interpolation method for large scale low frequency EM simulations," *IEEE Trans. Comput.-Aided Des. Integr. Circuits Syst.*, Vol. 24, No. 9, 1427–1443, Sep. 2005.
16. Wang, H. G. and C. H. Chan, "The implementation of multilevel Green's function interpolation method for full-wave electromagnetic problems," *IEEE Trans. Antennas Propag.*, Vol. 55, No. 5, 1348–1358, May 2007.
17. Wang, H. G., C. H. Chan, L. Tsang, and K. F. Chan, "Mixture

effective permittivity simulations using IMLMQRF method on preconditioned EFIE," *Progress In Electromagnetics Research*, PIER 57, 285–310, 2006.

18. Medgyesi-Mitschang, L. N. and J. M. Putnam, "Integral equation formulations for imperfectly conducting scatters," *IEEE Trans. Antennas Propag.*, Vol. 33, No. 2, 206–214, Feb. 1985.
19. Arbor, A., "A note on impedance boundary conditions," *Can. J. Phys.*, Vol. 40, 663–666, 1962.
20. Gilberg, R. F. and B. A. Forouzan, *Data Structures: A Pseudocode Approach with C++*, Thomson Asia Pte Ltd and PPTPH, 2002.
21. Pozar, D. M., *Microwave Engineering*, 2nd edition, Wiley, 1998.
22. Qian, Z. G., W. C. Chew, and R. Suaya, "Generalized impedance boundary condition for conductor modeling in surface integral equation," *IEEE Trans. Microw. Theory Tech.*, Vol. 55, No. 11, 2354–2364, Nov. 2007.
23. Zhao, J. S. and W. C. Chew, "Integral equation solution of Maxwell's equations from zero frequency to microwave frequencies," *IEEE Trans. Antennas Propagat.*, Vol. 48, No. 10, 1635–1645, Oct. 2000.
24. Cui, T. J. and W. C. Chew, "Accurate analysis of wire structures from very-low frequency to microwave frequency," *IEEE Trans. Antennas Propagat.*, Vol. 50, No. 3, 301–307, Mar. 2002.
25. Li, M.-K. and W. C. Chew, "Applying divergence-free condition in solving the volume integral equation," *Progress In Electromagnetics Research*, PIER 57, 311–333, 2006.
26. Rao, S. M., D. R. Wilton, and A. W. Glisson, "Electromagnetic scattering by surfaces of arbitrary shape," *IEEE Trans. Antennas Propagat.*, Vol. 30, No. 3, 409–418, May 1982.
27. Hussein, K. F. A., "Fast computational algorithm for EFIE applied to arbitrarily-shaped conducting surfaces," *Progress In Electromagnetics Research*, PIER 68, 339–357, 2007.
28. Hänninen, I., M. Taskinen, and J. Sarvas, "Singularity subtraction integral formulae for surface integral equations with RWG, ROOFTOP and hybrid basis functions," *Progress In Electromagnetics Research*, PIER 63, 243–278, 2006.
29. Kamon, M., M. J. Tsuk, and J. K. White, "FASTHENRY: A multipole accelerated 3-D inductance extraction program," *IEEE Trans. Microw. Theory Tech.*, Vol. 42, No. 9, 1750–1758, Sep. 1994.